

# Simultaneously High Gravimetric and Volumetric Gas Uptake Characteristics of the Metal–Organic Framework NU-111

Yang Peng,<sup>a,b</sup> Gadipelli Srinivas<sup>a,b</sup>, Christopher E. Wilmer,<sup>c</sup> Ibrahim Eryazici,<sup>d</sup> Randall Q. Snurr,<sup>c</sup>  
Joseph T. Hupp<sup>d</sup>, Taner Yildirim,<sup>a,b,\*</sup> and Omar K. Farha<sup>d,\*</sup>

*Institutions:*

<sup>a</sup>NIST Center for Neutron Research, National Institute of Standards and Technology, Gaithersburg, Maryland, 20899-6102 (USA).

<sup>b</sup>Department of Materials Science and Engineering, University of Pennsylvania, Philadelphia, Pennsylvania, 19104-6272 (USA).

<sup>c</sup>Department of Chemical and Biological Engineering, Northwestern University, 2145 Sheridan Road, Evanston, Illinois 60208 (USA).

<sup>d</sup>Department of Chemistry and International Institute for Nanotechnology, Northwestern University, 2145 Sheridan Road, Evanston, Illinois 60208 (USA).

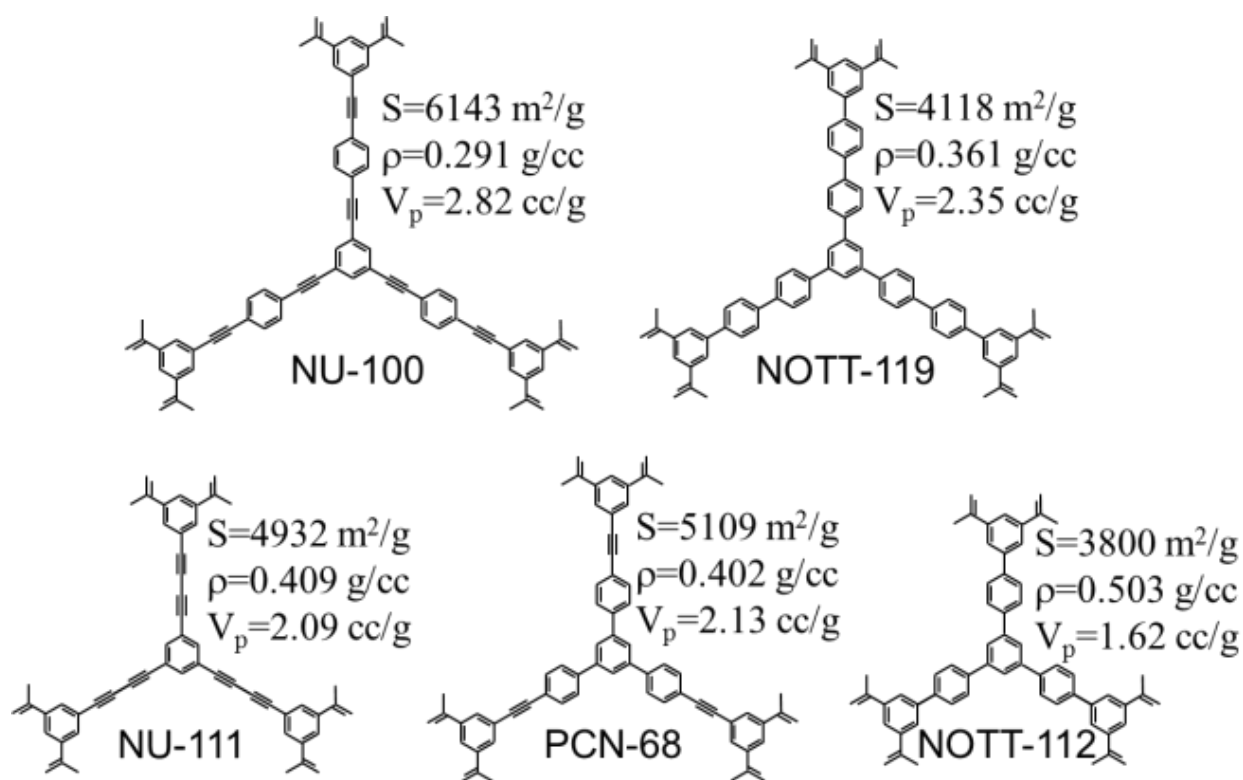
\* Corresponding authors: [taner@seas.upenn.edu](mailto:taner@seas.upenn.edu) and [o-farha@northwestern.edu](mailto:o-farha@northwestern.edu)

## Table of Contents

<b>Section S1.</b> Linkers Used in 2 <sup>nd</sup> Generation MOFs with Very Large Surface Area	S2
<b>Section S2.</b> Nitrogen Isotherms	S3
<b>Section S3.</b> Volumetric High-Pressure Adsorption Measurements and Excess Isotherms on NU-111	S4-S7
<b>Section S4.</b> Measured Isothermic Heat of Adsorption Q <sub>st</sub>	S8-S10
<b>Section S5.</b> Simulated High-Pressure Adsorption of NU-111	S11–S13
<b>Section S6.</b> X-ray pattern and crystal structure of NU-111	S13-15
<b>Section S7.</b> References	S15

## Section S1. Linkers Used in 2<sup>nd</sup> Generation MOFs with Very Large Surface Area

Recently significant advances have been made in synthesizing new MOFs with record high internal surface areas and pore volumes exceeding 4000 m<sup>2</sup>/g and 2 cc/g by utilizing longer organic linkers and copper paddlewheel as the open metal sites. Some of these linkers and the names of the corresponding MOFs are shown in Scheme 1: PCN-68/NOTT-116, PCN-69/NOTT-119, NOTT-112, NU-100/PCN-610, and NU-111.



**Scheme 1** Hexacarboxylic acid struts used to construct NU-100/PCN-610, NOTT-119/PCN-69, NU-111, PCN-68/NOTT-116, and NOTT-112. Surface area, crystal density and pore volume of each MOF are also given.

## Section S2. Nitrogen Isotherms

First, we studied the permanent porosity of activated NU-111 by N<sub>2</sub> adsorption measurements at 77 K (Figure S1). By applying the Brunauer-Emmett-Teller (BET) model in the pressure range  $P/P_0 = 0.02 \sim 0.14$ , the specific surface area of NU-111 was calculated to be 4930 m<sup>2</sup>/g (see inset in Figure S1), which agrees well with the value obtained from a simulated N<sub>2</sub> isotherm of 4915 m<sup>2</sup>/g. This is one of the few MOFs with a BET surface area exceeding 3800 m<sup>2</sup>/g. NU-111 exhibits exceptionally high N<sub>2</sub> uptake of 1350 cc/g at saturation and a pore volume based on the maximum of N<sub>2</sub> adsorption of 2.09 cc/g. The experimental pore volume is in excellent agreement with the value calculated from PLATON (2.03 cc/g).

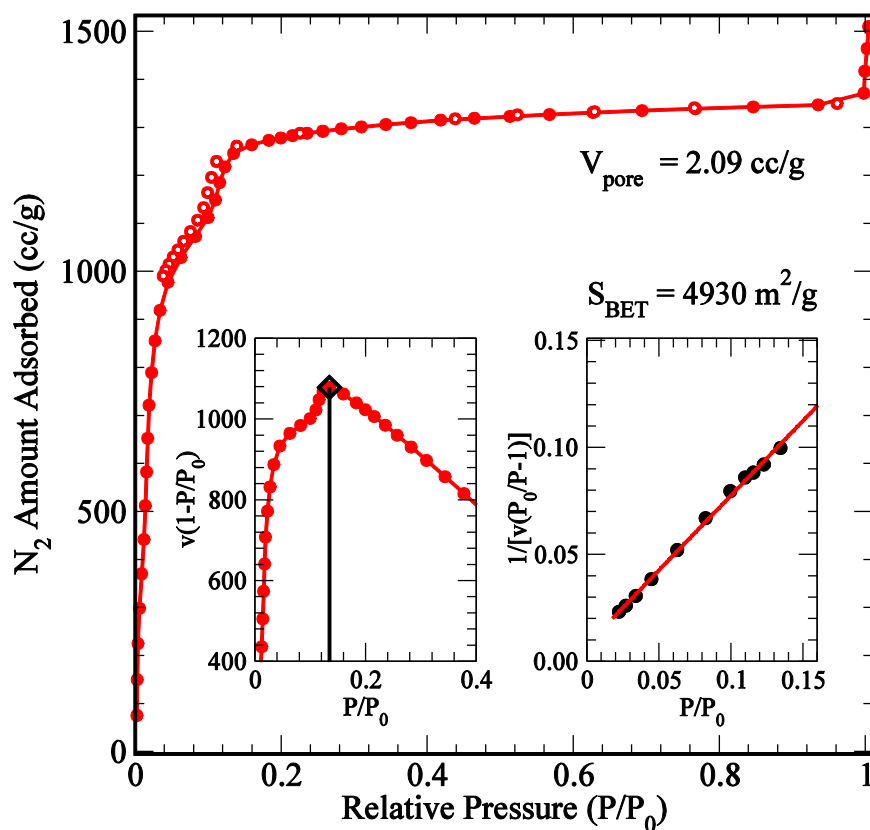


**Figure S1.** N<sub>2</sub> adsorption isotherm at 77 K. The inset on the left shows the consistency plot to determine the pressure range for BET fitting<sup>2</sup>, which is shown in the right inset.

### Section S3. Volumetric High-Pressure Adsorption Measurements and Excess Isotherms on NU-111.

Based on the widely used volumetric method, we developed a fully computer-controlled Sieverts apparatus as discussed in detail in Ref. 1. Briefly, our fully computer controlled Sievert apparatus operates in a sample temperature range of 20 K to 500 K and a pressure range of 0 to 100 bar. In the volumetric method, gas is admitted from a dosing cell with known volume to the sample cell in a controlled manner; the gas pressure and temperature are controlled and recorded. Some unique features of our setup are as follows. We have five gas inlets including He, N<sub>2</sub>, CO<sub>2</sub>, CH<sub>4</sub>, and H<sub>2</sub>, enabling us to perform first nitrogen pore volume and surface measurements and then He-cold volume determination and then the gas adsorption measurements without moving the sample from the cell and using the same protocol. We use four pressure gauges with four different pressure ranges (20, 100, 500 and 3000 psi respectively) to precisely measure the pressure. For isotherm measurement below room temperature, the sample temperature is controlled using a closed cycle refrigerator (CCR). The difference between the real sample temperature and the control set-point is within 1 K in the whole operating temperature range. The connection between the sample cell and the dose cell is through 1/8'' capillary tubing, which provides a sharp temperature interface between the sample temperature and the dose temperature (i.e., room temperature).

The cold volumes for the empty cell were determined using He as a function of pressure at every temperature before the real sample measurement and were used to calculate the sample adsorption. In parallel to these empty cell based isotherms, we also measured isotherms using He gas and sample in the cell. Assuming He-adsorption is small, this method is more accurate. As shown in the Figure below, the isotherms from both methods (i.e. empty cell cold volume, and He-cold volume with the sample) agree with each other reasonably well. As a third cross check of our measurements, we repeated all the isotherms on an empty cell with the same gas and temperatures. Using previously measured cold volumes, we verify that the empty cell does not appear to show any adsorption. Based on this empty cell adsorption measurement, the error bars in our isotherms are around 1% at 35 bar and at most 2-3 % at 60 bar.

In the paper (and below), we compare the absolute (and excess) isotherms obtained from He-runs (orange color) and the blank empty cell runs (black). For practical purposes, the two methods result in basically very similar isotherms, giving us confidence about the measurements and some idea about the error bars. The biggest difference is at 200 and 240 K where He-runs give lower isotherms. This is what we expect. At these temperatures and at high pressures, some He will be adsorbed in the sample, which results in a slightly larger cold-volume and therefore lower adsorption. At high temperatures, He-runs seem to give slightly higher isotherms than empty cell runs. The difference is about 1-3 percent.

Since the adsorbed amount is deducted from the raw *P-V-T* data using a real gas equation of state, a critically important issue is the accuracy of the chosen equation of state (EOS) in terms of describing the real gas behavior within the desired temperature and pressure range. We found that the simple EOS such as van der Waals (vdW) EOS works well at only ambient pressure and temperature, while it cannot describe the real gas behavior at low temperature and high pressure. Alternatively, for small gas molecules, the modified Benedict-Webb-Rubin (MBWR) EOS

seems to work well over a wide temperature and pressure range. Using an empty cell as a reference, we found that the MBWR EOS best describes the real gas behavior of He, H<sub>2</sub> and CH<sub>4</sub>. Therefore, in all our isotherm data reduction, the NIST MBWR EOS is used. [*NIST Standard Reference Database 23: NIST Reference Fluid Thermodynamic and Transport Properties Database*].

Finally, we note that we repeated both CH<sub>4</sub> and CO<sub>2</sub> isotherms at room temperature several times over a period of six months and did not see any evidence of sample degradation. We believe that as long as the sample is kept in an inert atmosphere such as in He-glove box, it is very stable and many cycles of adsorption of CO<sub>2</sub>/CH<sub>4</sub> do not seem to have any effect on the adsorption uptake capacity.

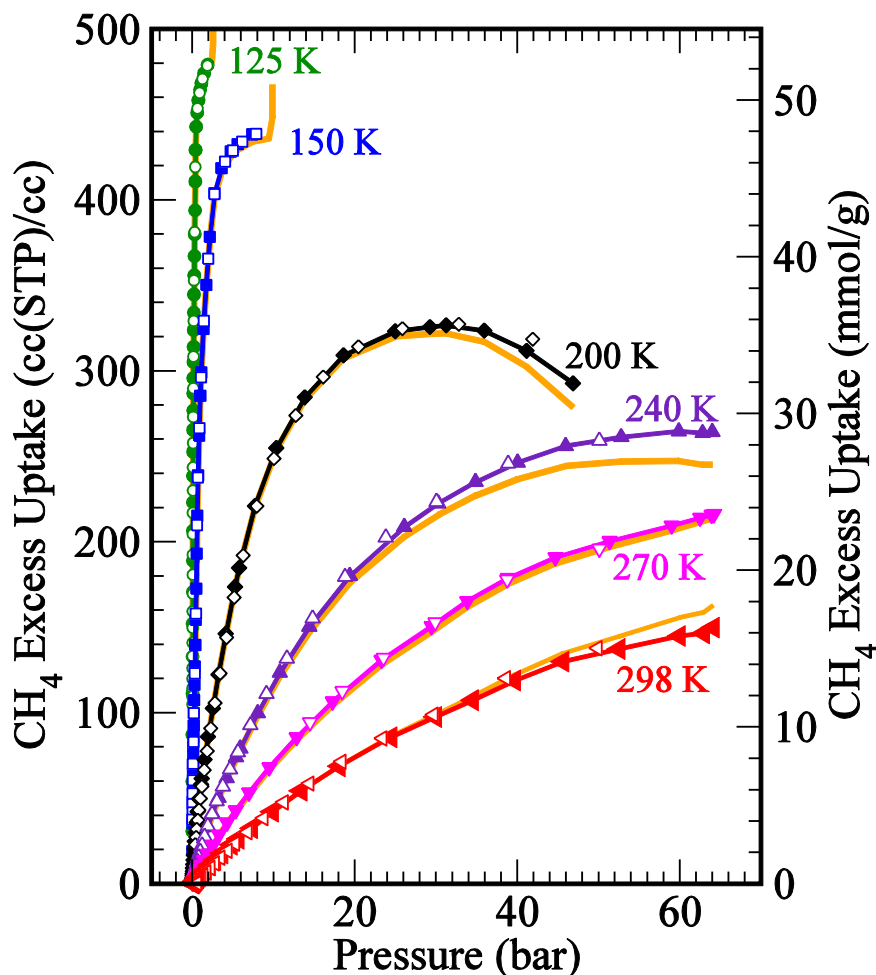


**Figure S2.** The excess isotherms for CH<sub>4</sub> at various temperatures. The corresponding total isotherms are shown and discussed in the text. The total (i.e. absolute) isotherms were obtained from excess isotherms by adding the amount of gas in the pore volume at the measured pressure and temperature (using the NIST MBWR real gas equation). We used the measured pore volume from the nitrogen isotherm. The orange color lines represent isotherms obtained from He-cold volume with sample in while the other isotherms are using empty-cell void volumes. The difference is due to adsorption of He by the sample. Open symbols indicate desorption isotherms.

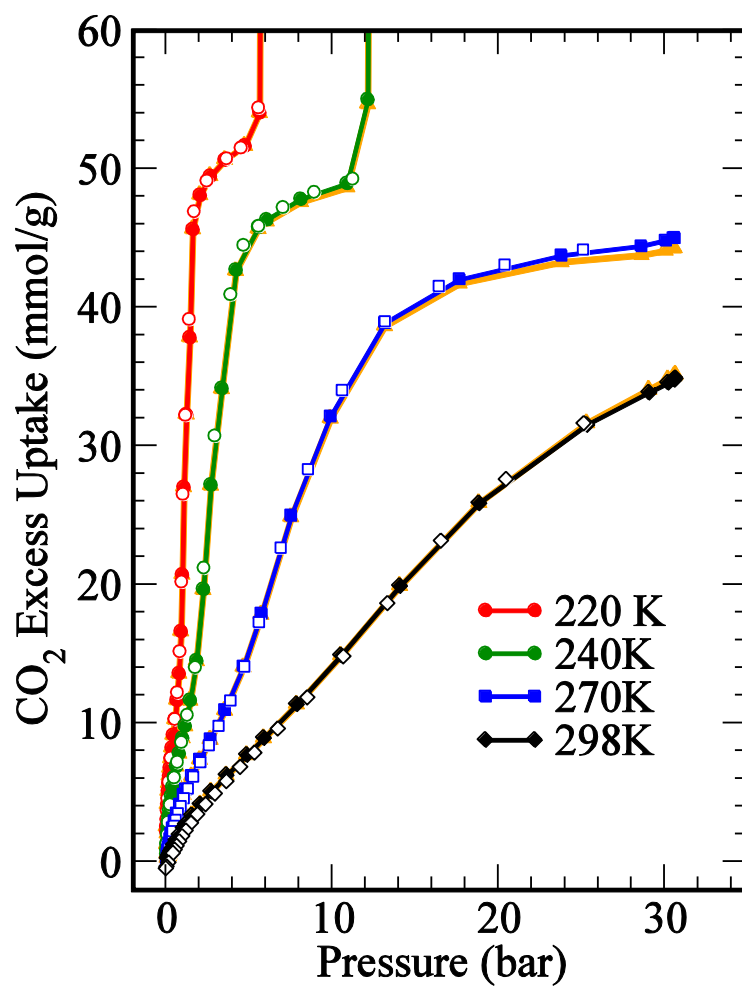
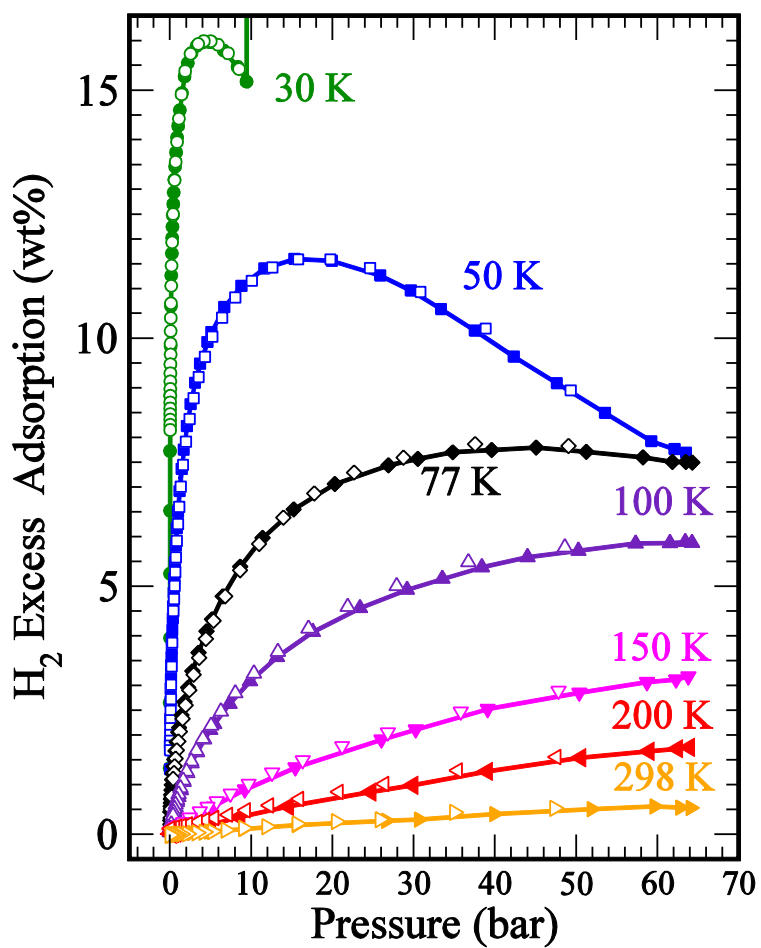


Figure S3. Same as Fig. S2 but for CO<sub>2</sub>.



**Figure S4.** Excess isotherms for H<sub>2</sub> at various temperatures.

#### Section S4. Measured Isothermic Heat of Adsorption $Q_{st}$

Our isotherm data at a series of temperatures (Fig. 2 of the main text) enable us to extract the heat of adsorption  $Q_{st}$  as a function of the adsorbed amount.  $Q_{st}$  is calculated using the “isosteric method” where a series of isotherms are measured at a wide range of temperatures. These isotherms are then parameterized by cubic-spline which does not require any fitting and allows us to interpolate the isotherm at a constant loading. Then, the  $Q_{st}$  is obtained from the  $\ln(P)$  versus  $1/T$  plots. As an alternative to cubic-spline interpolation, we also obtain  $Q_{st}$  by fitting the isotherm data using the following form of a virial equation:

$$\ln(p) = \ln(v) + \frac{1}{T} \sum_{i=0}^m a_i v^i + \sum_{i=0}^n b_i v^i$$

where  $v$ ,  $p$ , and  $T$  are the amount adsorbed, pressure, and temperature, respectively and  $a_i$  and  $b_i$  are empirical parameters. The first four constants (i.e.  $a_0$ ,  $b_0$ ,  $a_1$ , and  $b_1$ ) are obtained by linearizing the isotherms ( $1/n$  versus  $\ln p$ ) and then we increase the number of parameters gradually (two at a time) until the improvement in the fit is not significant. Usually 10 or 12 parameters are found to be enough to obtain a good fit to the isotherms. After the isotherms are fitted, by applying Clausius-Clapeyron equation, the heat of adsorption is obtained as

$$Q_{st} = -R \sum_{i=0}^m a_i v^i$$

where  $R$  is the universal gas constant. The details can be found in [Jagiello *et al*, *J. Chem. Eng. Data*, 1995; **40**; 1288-92 and Jagiello *J at al*, *Langmuir* 1996, **12**,2837-42].

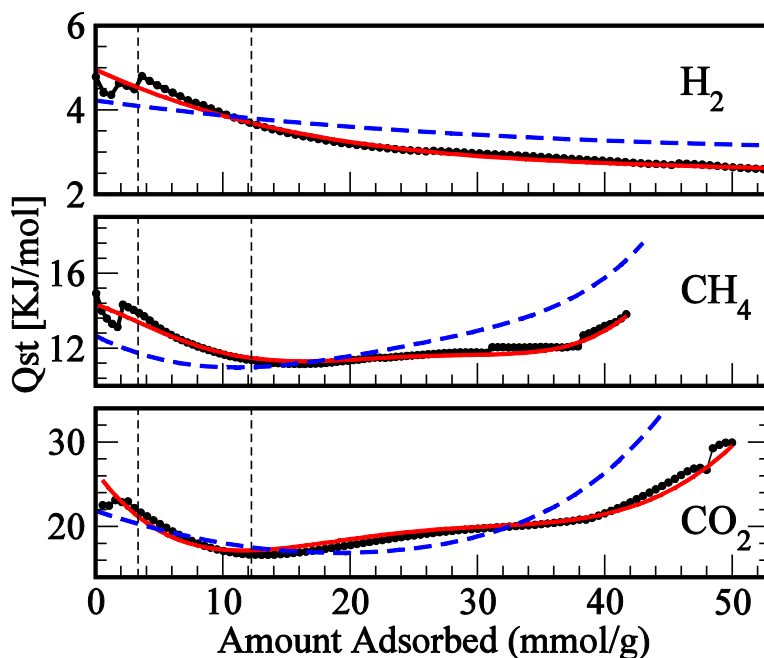


**Figure S5.** Isothermic heats of adsorption for  $H_2$ ,  $CH_4$  and  $CO_2$ . The red and black lines are from experimental data using spline and virial fitting, respectively. The blue dashed lines represent  $Q_{st}$  values determined from the simulated isotherms.

As an example, below we show the isotherm data (points), cubic-spline interpolation (solid lines) and the virial-fit (dotted lines) as well as the corresponding  $\ln(P)$  versus  $1/T$  plots and the  $Q_{st}$  from both methods along with the fit parameters  $a_i$  and  $b_i$ .

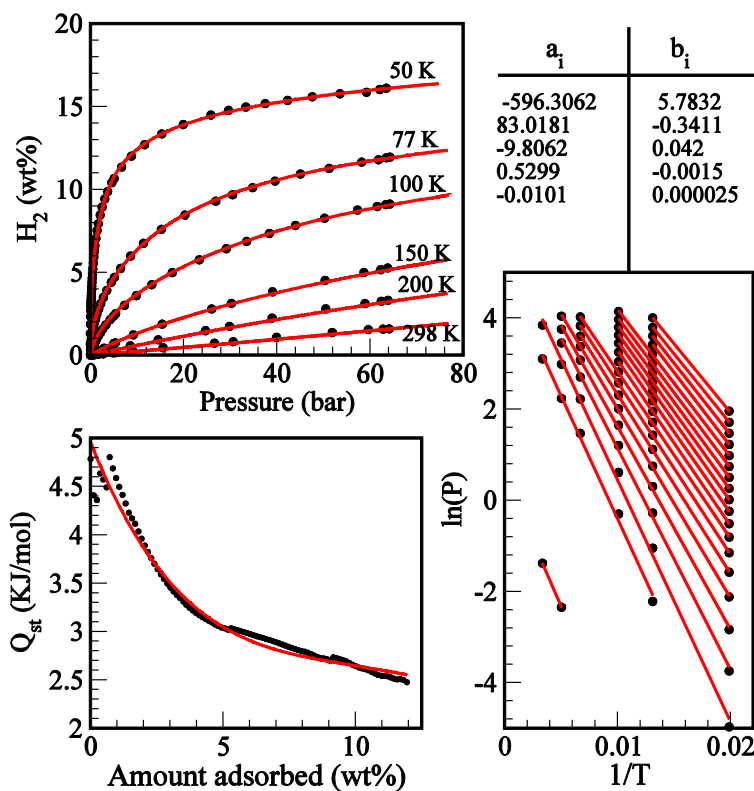


**Figure S6.** The H<sub>2</sub> adsorption isotherms (dots) and the virial fit (red-lines) along with the fit parameters as well as the  $Q_{st}$  and the  $\ln(P)$ - $1/T$  plots. The black line in the  $Q_{st}$  plot is obtained from the raw-data without any virial fitting (using spline method).

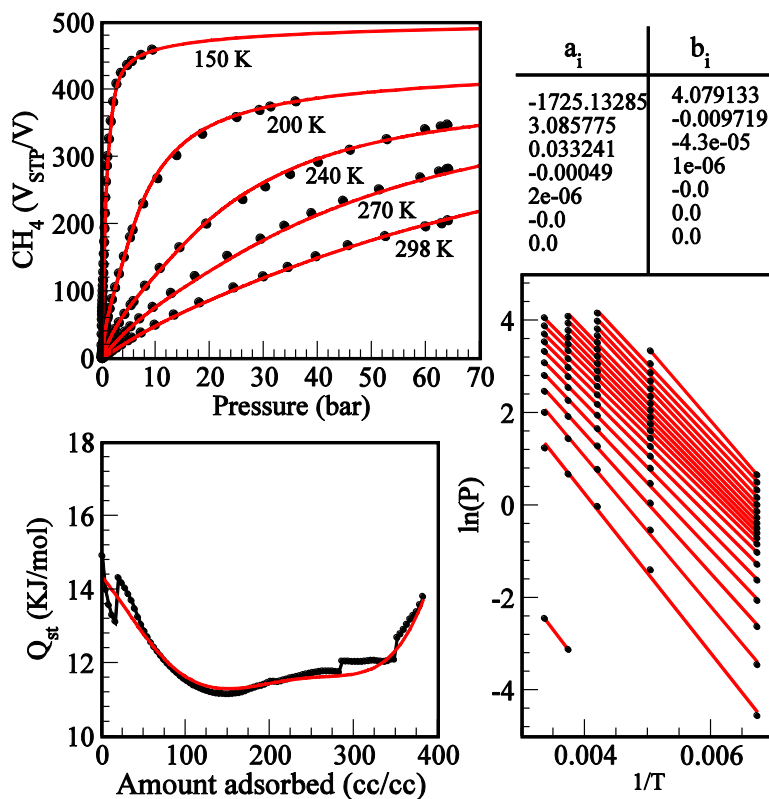


Figure S7. Same as Fig. S6 but for CH<sub>4</sub> adsorption.

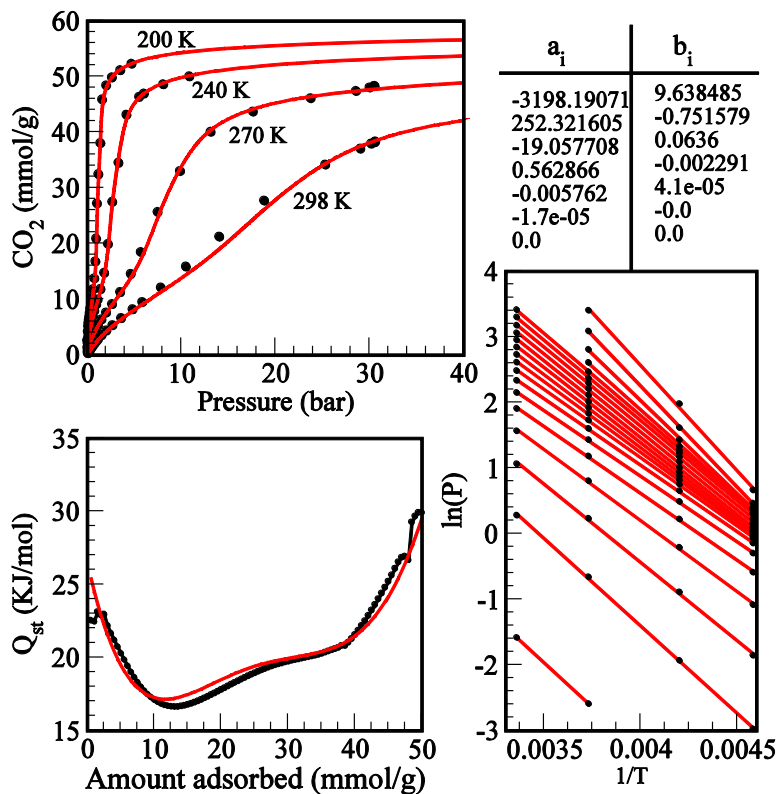


Figure S8. Same as Fig. S6 but for CO<sub>2</sub> adsorption.

## Section S5. Simulated High-Pressure Adsorption of NU-111

Atomistic grand canonical Monte Carlo (GCMC) simulations were performed to estimate the adsorption isotherms of N<sub>2</sub>, CH<sub>4</sub>, CO<sub>2</sub> and H<sub>2</sub> in NU-111.

**Interaction potential.** For simulations of N<sub>2</sub>, CH<sub>4</sub>, and CO<sub>2</sub> adsorption, interaction energies between non-bonded atoms were computed through a Lennard-Jones (LJ) + Coulomb potential:

$$\mathcal{V}_{ij} = 4\epsilon_{ij} \left( \left( \frac{\sigma_{ij}}{r_{ij}} \right)^{12} - \left( \frac{\sigma_{ij}}{r_{ij}} \right)^6 \right) + \frac{q_i q_j}{4\pi\epsilon_0 r_{ij}}$$

where  $i$  and  $j$  are interacting atoms, and  $r_{ij}$  is the distance between atoms  $i$  and  $j$ ,  $\epsilon_{ij}$  and  $\sigma_{ij}$  are the LJ well depth and diameter, respectively,  $q_i$  and  $q_j$  are the partial charges of the interacting atoms, and  $\epsilon_0$  is the dielectric constant. LJ parameters between different types of sites were calculated using the Lorentz-Berthelot mixing rules.

For simulations of H<sub>2</sub> adsorption at 77 K, quantum diffraction effects become important, which can be accounted for using the quasiclassical Feynman-Hibbs (FH) potential.<sup>3,4</sup> We modeled hydrogen at this temperature as follows:

$$\mathcal{V}_{ij} = 4\epsilon_{ij} \left( \left( \frac{\sigma_{ij}}{r_{ij}} \right)^{12} - \left( \frac{\sigma_{ij}}{r_{ij}} \right)^6 \right) + \overbrace{\frac{4\epsilon_{ij}}{r_{ij}^2} \frac{\hbar^2}{24\mu_{ij}k_B T} \left( 132 \left( \frac{\sigma_{ij}}{r_{ij}} \right)^{12} - 30 \left( \frac{\sigma_{ij}}{r_{ij}} \right)^6 \right)}^{\text{FH Correction}} + \frac{q_i q_j}{4\pi\epsilon_0 r_{ij}}$$

where  $\mu_{ij}$  is the reduced mass,  $m_i m_j / (m_i + m_j)$  of the two interacting atoms having atomic masses  $m_i$  and  $m_j$ ,  $T$  is the temperature, and  $k_B$  and  $\hbar$  are Boltzmann's constant and Planck's constant, respectively. For comparison, we also ran simulations without the middle Feynman-Hibbs "correction" term.

**MOF models.** LJ parameters for the framework atoms were taken from the Universal Force Field (UFF).<sup>5</sup> Partial charges were determined using the extended charge equilibration (EQeq) algorithm developed by Wilmer et al.,<sup>6</sup> assuming neutral charge centers for all atoms except Cu, for which a +2 charge center was used, and assuming a global relative dielectric permittivity of 1.67. Table S2 shows the LJ parameters for framework atom types found in NU-111.

**Table S2.** LJ parameters for framework atoms in NU-111 taken from the UFF force field.

Atom type	$\sigma$ (Å)	$\epsilon/k_B$ (K)
C	3.43	52.83
O	3.12	30.19
H	2.57	22.14
Cu	3.114	2.516
N	3.261	34.721

**Nitrogen Model.** Nitrogen molecules were modeled using the TraPPE force field,<sup>7</sup> which was originally fit to reproduce the vapor-liquid coexistence curve of nitrogen. In this force field, the nitrogen molecule is a rigid structure where the N-N bond length is fixed at its experimental value of 1.10 Å. This model reproduces the experimental gas-phase quadrupole moment of nitrogen by placing partial charges on N atoms and on a point located at the center of mass (COM) of the molecule. Table S3 shows the LJ parameters and partial charges for nitrogen.

**Table S3.** LJ parameters and partial charges for the sites in the nitrogen molecule.

Atom type	$\sigma$ (Å)	$\epsilon/k_B$ (K)	$q$ (e)
N	3.31	36.0	-0.482
N <sub>2</sub> COM	0	0	0.964

**Methane model.** The methane molecules were modeled using the TraPPE force field,<sup>8</sup> which was originally fit to reproduce the vapor-liquid coexistence curve of methane. In this force field, methane is modeled as a single sphere with the parameters shown in Table S5.

**Table S4.** LJ parameters for methane molecules.

Atom type	$\sigma$ (Å)	$\epsilon/k_B$ (K)	$q$ (e)
CH <sub>4</sub> (united)	3.75	148.0	---

**Carbon dioxide model.** Partial charges and LJ parameters for CO<sub>2</sub> were taken from the TraPPE force field.<sup>7</sup> This force field has been fit to reproduce the vapor-liquid coexistence curves by Siepmann and co-workers. The CO<sub>2</sub> molecule is modeled as a rigid and linear structure. Table S5 shows the LJ parameters and partial charges for CO<sub>2</sub>.

**Table S5.** LJ parameters and partial charges for the sites in the carbon dioxide molecule.

Atom type	$\sigma$ (Å)	$\epsilon/k_B$ (K)	$q$ (e)
C	2.80	27.0	0.70
O	3.05	79.0	-0.35

**Hydrogen Model.** For the hydrogen molecules, we used the model of Levesque et al.<sup>9</sup> and ran simulations with the FH correction. In this model, the hydrogen molecule is a rigid structure where the H-H bond length is fixed at 0.74 Å. This model reproduces the experimental gas-phase quadrupole moment of hydrogen by placing partial charges on H atoms and on a point located at the center of mass (COM) of the hydrogen molecule. Table S6 shows the LJ parameters and partial charges for hydrogen.

**Table S6.** LJ parameters and partial charges for the sites in the hydrogen molecule.

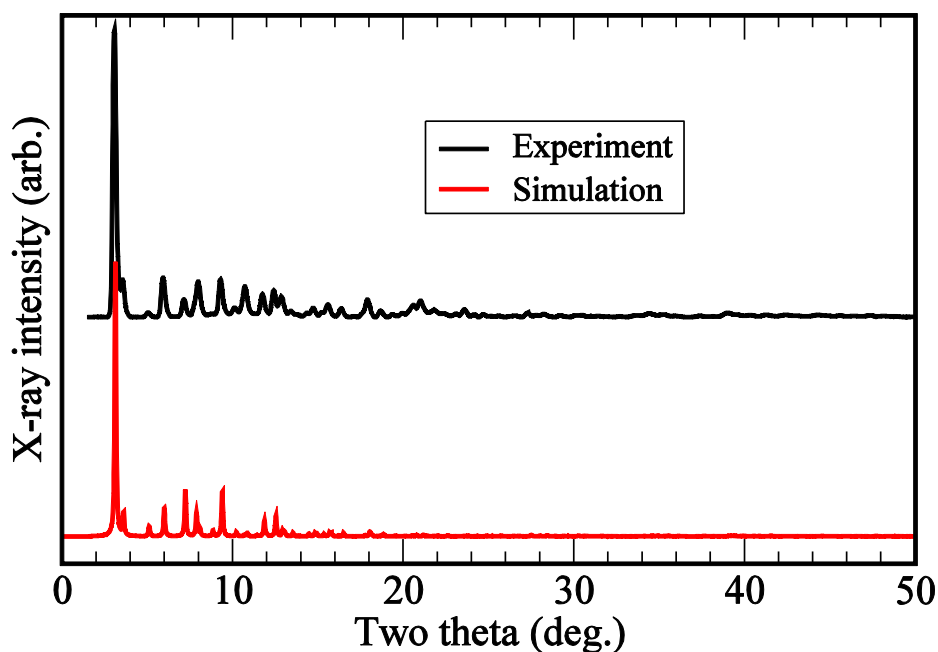
Atom type	$\sigma$ (Å)	$\epsilon/k_B$ (K)	$q$ (e)
H	0	0	0.468
H <sub>2</sub> COM	2.958	36.7	-0.936

**General GCMC simulation settings.** All GCMC simulations included a 2500-cycle equilibration period followed by a 2500-cycle production run. A cycle consists of  $n$  Monte Carlo steps, where  $n$  is equal to the number of molecules (which fluctuates during a GCMC simulation). All

simulations included random insertion/deletion, translation and rotation moves (except methane, where no rotation moves were used) of molecules with equal probabilities. Atoms in the MOF were held fixed at their crystallographic positions. An LJ cutoff distance of 12.0 Å was used for all simulations. The Ewald sum technique was used to compute the electrostatic interactions. One unit cell of **NU-111** was used for the simulations. N<sub>2</sub> isotherms were simulated at 77 K up to 0.398 bar. Fugacities needed to run the GCMC simulations were calculated using the Peng-Robinson equation of state.

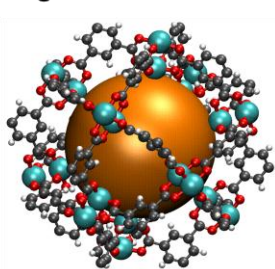
### Section S6. Crystallinity/X-ray diffraction and Nano-cages of NU-111 Structure

The synthesis, structure and crystallinity of NU-111 were recently reported in Ref. 10. Here we show the x-ray powder pattern of the NU-111 sample, indicating that it's highly crystalline.

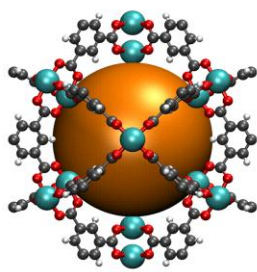


The NU-111 structure has a noncatenated face-centered-cubic (fcc) lattice, in which the framework nodes consist of Cu-paddlewheels coordinated by the carboxylates of the linkers. The overall structure can be viewed as the packing of four cages in a fcc lattice as shown below.

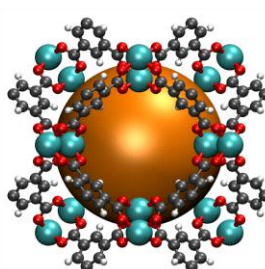
Cage 1



“Interesting” view

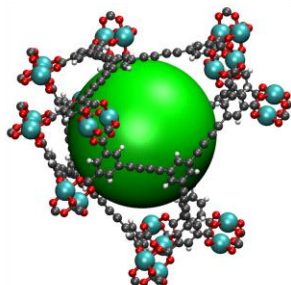


side view 1

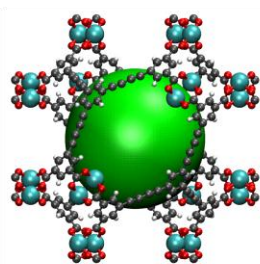


side view 2

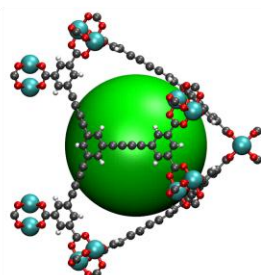
### Cage 2



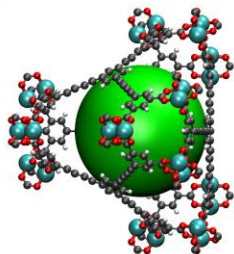
“Interesting”  
view



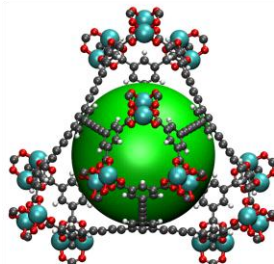
side view 1



side view 2

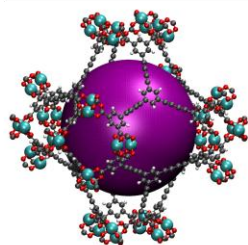


side view 1

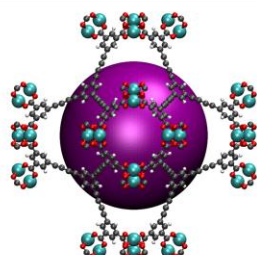


side view 2

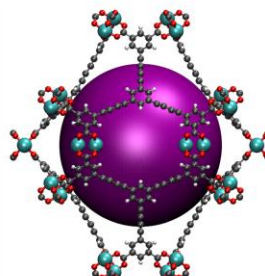
### Cage 3



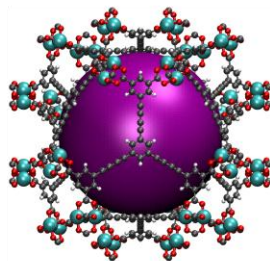
“Interesting”  
view



side view 1

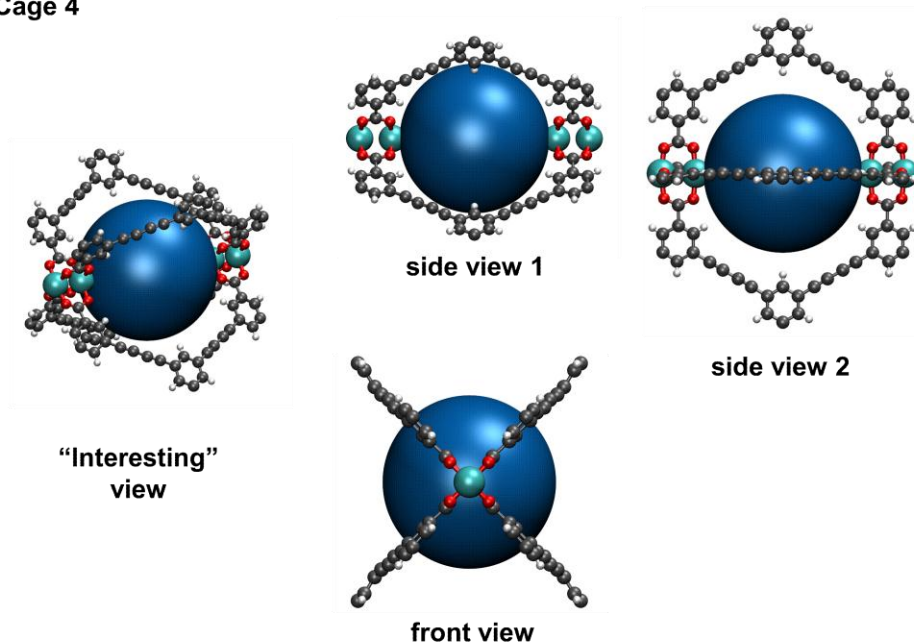


side view 2



side view 3

#### Cage 4



#### S7. Reference

1. W. Zhou, H. Wu, M. R. Hartman, and T. Yildirim, *J. Phys. Chem. C*, 2007, **111**, 16131–16137.
2. K. S. Walton and R. Q. Snurr, *J. Am. Chem. Soc.*, 2007, **129**, 8552–8556.
3. R. B. Getman, Y.-S. Bae, C. E. Wilmer, and R. Q. Snurr, *Chem. Rev.*, 2011, **112**, 703–723.
4. R. P. Feynman and A. R. Hibbs, *Quantum Mechanics and Path Integrals*, McGraw-Hill Companies, First edn., 1965.
5. A. K. Rappé, C. J. Casewit, K. S. Colwell, W. A. Goddard III, and W. M. Skiff, *J. Am. Chem. Soc.*, 1992, **114**, 10024–10035.
6. C. E. Wilmer, K.-C. Kim, and R. Q. Snurr, *J. Phys. Chem. Lett.*, 2012, **3**, 2506–2511.
7. J. J. Potoff and J. I. Siepmann, *AIChE J.*, 2001, **47**, 1676–1682.
8. M. G. Martin and J. I. Siepmann, *J. Phys. Chem. B*, 1998, **102**, 2569–2577.
9. D. Levesque, A. Gicquel, F. L. Darkrim, and S. B. Kayiran, *J. Phys.-Condes. Matter*, 2002, **14**, 9285–9293.
10. O. K. Farha, C.E. Wilmer, I. Eryazici, B. G. Hauser, P. A. Parilla, K. O’Neill, A. A. Sarjeant, S. T. Nguyen, R. Q. Snurr and J. T. Hupp, *J. Am. Chem. Soc.*, 2012, **134**, 9860.